Monthly Notices
of the
ROYAL ASTRONOMICAL SOCIETY

MNRAS **488,** 2332–2342 (2019)
Advance Access publication 2019 July 8

doi:10.1093/mnras/stz1856

ExoMol line list – XXXIV. A rovibrational line list for phosphinidene (PH) in its $X\,^3\Sigma^-$ and $a\,^1\Delta$ electronic states

Jonathan Langleben,[1] Jonathan Tennyson ,[1]★ Sergei N. Yurchenko[1] and Peter Bernath[2]

[1]*Department of Physics and Astronomy, University College London, London WC1E 6BT, UK*
[2]*Department of Chemistry and Biochemistry, Old Dominion University, 4541 Hampton Boulevard, Norfolk, VA 23529, USA*

Accepted 2019 July 2. Received 2019 June 30; in original form 2019 April 28

ABSTRACT

A rovibronic line list for the ground ($X\,^3\Sigma^-$) and first excited ($a\,^1\Delta$) states of phosphinidene, ^{31}PH, is computed. The line list is designed for studies of exoplanetary and cool stellar atmospheres with temperatures up to 4000 K. A combination of empirical and *ab initio* data is used to produce the line list: potential energy curves (PECs) are fitted using experimental transition frequencies; these transitions are reproduced with a root mean square error of 0.01 cm^{-1}. The nuclear Schrödinger equation is solved using these PECs plus Born–Oppenheimer and spin splitting correction terms. Line intensities and Einstein A coefficients are computed using *ab initio* dipole moment curves for X–X and a–a transitions. The resulting LaTY line list, which contains 65 055 transitions for 2528 rovibronic states up to 24 500 cm^{-1} and $J = 80$, is used to simulate spectra in emission and absorption for a range of temperatures. The line list is made available in electronic form at the CDS and ExoMol data bases.

Key words: molecular data – opacity – astronomical data bases: miscellaneous – planets and satellites: atmospheres – stars: low-mass.

1 INTRODUCTION

The biochemistry of living organisms is heavily dependent on phosphorus. It is important for the storage of genetic information in the form of DNA and RNA (nucleic acids) and is a key contributor to the structure of the cell membrane. The discovery of phosphorus-bearing species in the astrophysical arena is thus thought to be of great significance (Macia 2005; Cui et al. 2017; Zerkle 2018). There have been numerous astrophysical attempts to detect diatomic phosphorus molecules. To date, only PO (Tenenbaum, Woolf & Ziurys 2007), PN (Ziurys 1987), and CP (Guelin et al. 1990) have been identified in the interstellar medium or circumstellar shells. The discovery of PH has so far eluded astronomers (Hollis et al. 1980; Hjalmarson, Bergman & Biver 2004). However, models of both the interstellar medium (Thorne et al. 1984; Millar 1991) and (exo-) planetary atmospheres (Visscher, Lodders & Fegley 2006) suggest that there are environments where PH should be present in observable quantities. The purpose of this paper is to provide a comprehensive line list for PH to aid in its possible detection and modelling of its spectrum. This line list supplements those of other phosphorus-bearing molecules, namely PN (Yorke et al. 2014), PH_3 (Sousa-Silva et al. 2015), PO, and PS (Prajapat et al. 2017), produced as part of the ExoMol project (Tennyson & Yurchenko 2012).

The gound electronic state of PH, known as phosphinidene, is of $^3\Sigma^-$ symmetry. It is a singly bonded species so has a lower dissociation energy, of D_e(PH) ≈ 3.18(3) eV (Luo 2007; Rumble 2018) (see detailed discussion below), compared to the multiply bonded phosphorus species that have been detected in space: D_e(PN) ≈ 6.3 eV (Curry, Herzberg & Herzberg 1933), D_e(PO) ≈ 5.47 eV (Rao, Reddy & Rao 1981), and D_e(CP) ≈ 5.41 eV (Shi et al. 2012). The spectrum of PH has been well studied in the laboratory (Pearse & Fowler 1930; Ishaque & Pearse 1939; Rostas, Cossart & Bastien 1974; Davies, Russell & Thrush 1975; Di Stefano et al. 1978; Xuan et al. 1978; Ashfold, Dixon & Stickland 1984; Droege & Engelking 1984; Ohashi, Kawaguchi & Hirota 1984; Gustafsson et al. 1985; Ram & Bernath 1987, 1996; Beutel et al. 1996; Hughes & Brown 1997; Klisch et al. 1998; Di Stefano, Lenzi & Ricci 1999; Fitzpatrick et al. 2003) and its electronic structure has been the subject of a number of computational studies (Bruna et al. 1981; Senekowitsch et al. 1986; Park & Sun 1992; Goto & Saito 1993; Fitzpatrick et al. 2002; Jie-Min et al. 2012; Müller & Woon 2013; Gao & Gao 2014). As discussed below, a number of these works form key inputs to the present study.

2 METHOD

Our general methodology for constructing rotation–vibration line

★ E-mail: j.tennyson@ucl.ac.uk

© The Author(s) 2019.
Published by Oxford University Press on behalf of The Royal Astronomical Society. This is an Open Access article distributed under the terms of the Creative Commons Attribution License (http://creativecommons.org/licenses/by/4.0/), which permits unrestricted reuse, distribution, and reproduction in any medium, provided the original work is properly cited.

Downloaded from https://academic.oup.com/mnras/article-abstract/488/2/2332/5529411 by UCL (University College London) user on 31 July 2019

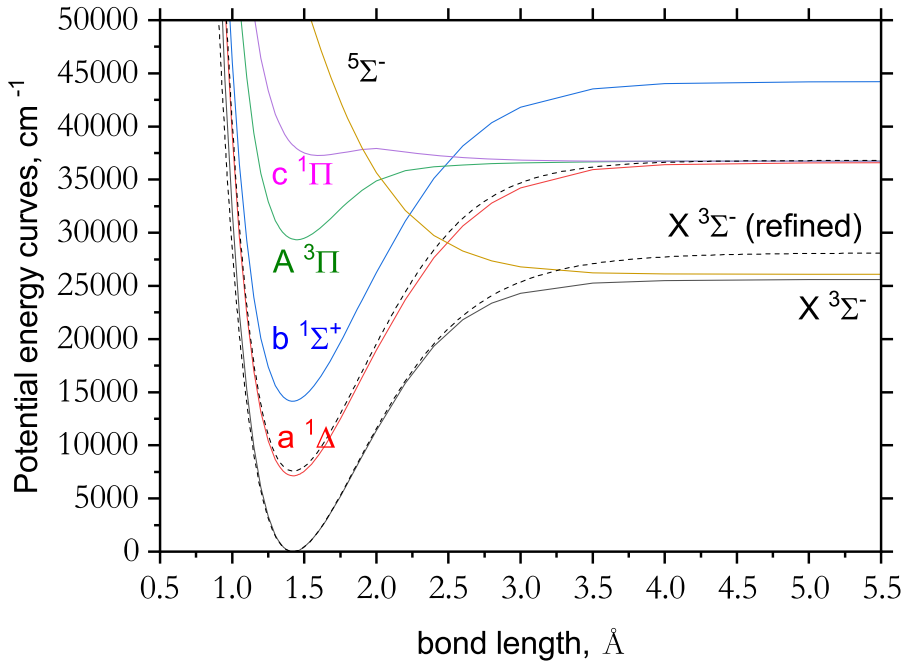

Figure 1. *Ab initio* PECs of the lowest electronic states of PH from Gao & Gao (2014) (solid lines) and the refined $X\,^3\Sigma^-$ and $a\,^1\Delta$ PECs from this work (dashed).

Table 1. Potential parameters defining empirical X and a PECs according to equation (1). The units are Å and cm^{-1}.

Parameters	PEC (X)	PEC(a)
V_e	0	7569
r_e	1.422179	1.423911
D_e	25 700	29 431
r_{ref}	1.422179	1.423911
p	4	4
N_L	1	1
N_R	5	4
β_0	1.7744781772	1.6765776631
β_1	0.1557401848	− 0.0443775470
β_2	0.0119350618	1.0241855379
β_3	0.4625698020	− 2.3099593616
β_4	− 0.8284568722	1.9917675261
β_5	0.9631507337	

lists is to use available experimental data to characterize the underlying potential energy curve but to use dipole moments computed *ab initio* (see Tennyson 2012; Tennyson & Yurchenko 2017). We follow this approach here. Since PH has a triplet electronic ground state, it is necessary to supplement this approach with spin coupling terms (Tennyson et al. 2016b). All nuclear motion calculations are performed with our general purpose, variational nuclear motion program for diatomic molecules, DUO (Yurchenko et al. 2016). We give details of this procedure in the remainder of this section.

2.1 Potential energy curve

The $X\,^3\Sigma^-$ and $a\,^1\Delta$ potential energy curves (PECs) were represented using the extended Morse oscillator (EMO) function as given by

$$V(r) = V_e + D_e\left[1 - \exp\left(-\sum_{k=0}^{N}\beta_k\xi_p^k(r - r_e)\right)\right]^2, \quad (1)$$

where D_e is the dissociation energy, ξ_p is the Šurkus variable given by

$$\xi_p = \left(\frac{r^p - r_{ref}^p}{r^p + r_{ref}^p}\right), \quad (2)$$

r_e is the corresponding equilibrium bond length, r_{ref} defines the expansion centre for the ξ_p variable (usually taken at r_e), and the integer value p influences how the function extrapolates beyond the data sensitive region. This form allows for extra flexibility in the degree of the polynomial on the left- or on the right-hand sides of the reference position, which is controlled by the parameters $N = N_L$ and N_R, respectively. The empirical parameters V_e and β_k are derived through refinement to experimental data via a least-squares fit, while the dissociation energies D_e are constrained to their experimental asymptotic energies $A_e = V_e + D_e$ (see discussion below).

A set of *ab initio* multireference configuration interaction with Davidson correction (MRCI+Q) curves for all low-lying states of PH from Gao & Gao (2014) is given in Fig. 1. We used their $X\,^3\Sigma^-$ and $a\,^1\Delta$ PECs as starting approximations for our model. As there was sufficient experimental data available for the ground electronic states of PH (Ram & Bernath 1987, 1996; Goto & Saito 1993; Klisch et al. 1998), the refined EMO PEC of fifth order was essentially determined by empirical refinement rather than from the *ab initio* curve of Gao & Gao (2014). For $a\,^1\Delta$, only the rotational lines for the (0,0) band, a–X electronic transition have been characterized (Beutel et al. 1996). Therefore only V_e and r_e parameters were refined, while all other parameters defining the corresponding EMO PEC of fourth order were fixed to their *ab initio* values. The final set of potential parameters is listed in Table 1.

Downloaded from https://academic.oup.com/mnras/article-abstract/488/2/2332/5529411 by UCL (University College London) user on 31 July 2019

Table 2. Expansion parameters defining spin–spin (SS), rotational Born–Oppenheimer breakdown (BOB), and spin–rotation (SR) functional forms according to equations (3) and (4). The bond length is in Å, the SS and SR functions are in cm^{-1}, and the BOB expansions are unitless.

Equation (4)	SS (X)	BOB (X)	Equation (3)	BOB (a)	SR (X)
r_{ref}	1.42218	1.42218	r_{ref}	1.42	1.42
γ_2	0.8	0.8	p	4	4
γ_4	0	0	C_0	0.0047811183	−0.0797377811
p	2	2	C_∞	0	0
C_0	1.4728278045	− 0.0001063699			
C_1	1.0957652053	0.0089251295			
C_2	0.4850903021	− 0.3045117774			
C_3	0	0.3645474486			
C_4	0	− 0.3901575147			
C_∞	0	0			

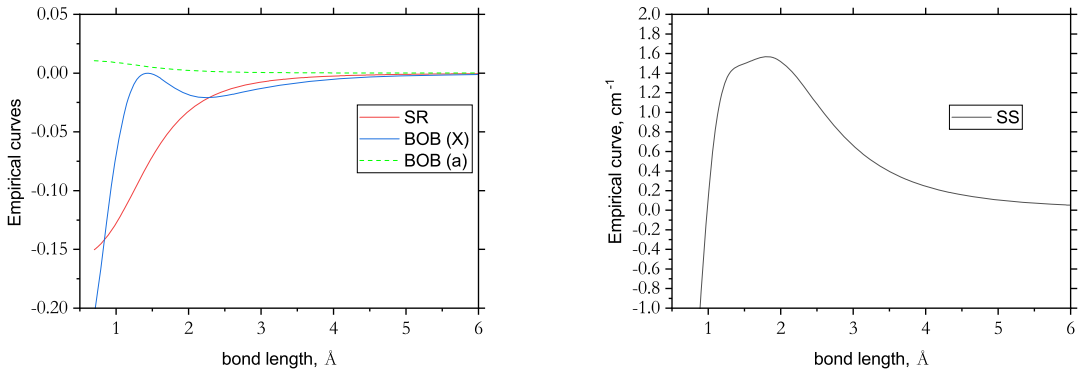

Figure 2. Empirical curvesof the $X\,^3\Sigma^-$ state of PH from in this work: spin–spin (cm^{-1}), spin–rotation (cm^{-1}), and Born–Oppenheimer breakdown (unitless).

Table 3. A comparison of experimentally derived vibrational energy levels (in cm^{-1}) for the $X\,^3\Sigma^-$ state of ^{31}PH from Ram & Bernath (1996) (Obs.) with those calculated using DUO (Calc.).

v	Obs.	Calc.	Obs. − Calc.
1	2276.20901(51)	2276.2061	0.00291
2	4465.02033(74)	4465.0148	0.00553
3	6566.15898(88)	6566.1561	0.00288
4	8578.9443(11)	8578.9506	− 0.0063
5	10502.1949(13)	10 502.2006	− 0.0057

Different couplings and corrections were modelled using the expansion

$$F(r) = (1 - \xi_p) \sum_{k=0}^{N} C_k\, z^k + \xi_p\, C_\infty, \tag{3}$$

where z is either taken as the Šurkus variable $z = \xi_p$ or using the damped-coordinate z given by

$$z = (r - r_{ref})\, e^{-\gamma_2 (r - r_{ref})^2 - \gamma_4 (r - r_{ref})^4} \tag{4}$$

(see also Prajapat et al. 2017; Yurchenko et al. 2018). Here p (integer), C_k, and C_∞ are adjustable parameters. The expansion centre r_{ref} is typically chosen to be close to the equilibrium value of the ground electronic state. To allow for rotational Born–Oppenheimer breakdown (BOB) effects (Le Roy 2017), which

Table 4. A comparison of experimental submillimetre frequencies (in cm^{-1}) for the $X\,^3\Sigma^-$ state of ^{31}PH from Goto & Saito (1993) and Klisch et al. (1998) (Obs.) with those calculated using DUO (Calc.).

J'	$\pm'$	e/f'	N'	J''	$\pm''$	e/f''	N''	Obs.	Calc.	Obs. − Calc.
0	+	e	1	1	−	e	0	14.1191	14.1185	0.0006
1	+	f	1	1	−	e	0	18.4634	18.4623	0.0011
2	+	e	1	1	−	e	0	16.4813	16.4811	0.0002
1	−	e	2	1	+	f	1	30.9308	30.9299	0.0009
1	−	e	2	0	+	e	1	35.2757	35.2738	0.0019
2	−	f	2	1	+	f	1	33.6363	33.6336	0.0027
2	−	f	2	2	+	e	1	35.6146	35.6148	− 0.0002
3	−	e	2	2	+	e	1	33.4474	33.4445	0.0029

Downloaded from https://academic.oup.com/mnras/article-abstract/488/2/2332/5529411 by UCL (University College London) user on 31 July 2019

Table 5. A comparison of experimental IR frequencies (in cm^{-1}) for the $X\,^3\Sigma^-$ state of ^{31}PH from Ram & Bernath (1987) (Obs.) with those calculated using DUO (Calc.) for a selection of transitions.

J'	$\pm'$	e/f'	v'	N'	J''	$\pm''$	e/f''	v''	N''	Obs.	Calc.	Obs. − Calc.
0	+	e	1	1	1	−	e	0	2	2240.4245	2240.4228	0.0017
0	+	e	2	1	1	−	e	1	2	2154.0349	2154.0248	0.0101
0	+	e	3	1	1	−	e	2	2	2067.3792	2067.3730	0.0062
1	−	e	1	2	0	+	e	0	1	2309.9615	2309.9625	−0.0010
1	−	e	1	0	2	+	e	0	1	2259.7221	2259.7249	−0.0028
1	+	f	1	1	2	−	f	0	1	2242.0659	2242.0688	−0.0029
1	−	e	1	2	2	+	e	0	3	2223.9221	2223.9240	−0.0019
1	−	e	2	0	2	+	e	1	1	2172.8223	2172.8137	0.0086
1	+	f	2	1	2	−	f	1	1	2155.6753	2155.6634	0.0119
1	−	e	2	2	2	+	e	1	3	2138.0416	2138.0324	0.0092
1	−	e	3	0	2	+	e	2	1	2085.6489	2085.6481	0.0008
1	+	f	3	1	2	−	f	2	1	2069.0122	2069.0003	0.0119
1	−	e	3	2	2	+	e	2	3	2051.8808	2051.8782	0.0026
...												
5	+	f	3	5	6	−	f	2	5	1999.0172	1999.0052	0.0120
5	−	e	3	6	6	+	e	2	7	1980.2734	1980.2631	0.0103
5	−	e	4	4	4	+	e	3	3	2068.7136	2068.7384	−0.0248
5	+	f	4	5	4	−	f	3	3	2081.4480	2081.4679	−0.0199
5	−	e	4	6	4	+	e	3	5	2093.6318	2093.6574	−0.0256
5	−	e	4	4	6	+	e	3	5	1931.4560	1931.4863	−0.0303
5	+	f	4	5	6	−	f	3	5	1913.6358	1913.6587	−0.0229
5	−	e	4	6	6	+	e	3	7	1895.3895	1895.4050	−0.0155
5	−	e	5	4	4	+	e	4	3	1977.0756	1977.0671	0.0085
5	+	f	5	5	4	−	f	4	3	1989.2557	1989.2403	0.0154
5	−	e	5	6	4	+	e	4	5	2000.8809	2000.8782	0.0027
6	+	e	1	5	5	−	e	0	4	2352.4659	2352.4577	0.0082
6	−	f	1	6	5	+	f	0	4	2366.1885	2366.1869	0.0016
...												
10	+	e	2	11	11	−	e	1	12	1962.6171	1962.6219	−0.0048
10	+	e	3	9	9	−	e	2	8	2219.3963	2219.3746	0.0217
10	−	f	3	10	9	+	f	2	8	2229.7211	2229.7033	0.0178
10	+	e	3	11	9	−	e	2	10	2239.4441	2239.4372	0.0069
10	+	e	3	9	11	−	e	2	10	1922.0451	1922.0214	0.0237
10	−	f	3	10	11	+	f	2	10	1901.6330	1901.6003	0.0327
10	+	e	3	11	11	−	e	2	12	1880.8366	1880.8019	0.0347
10	+	e	4	9	9	−	e	3	8	2126.2936	2126.3060	−0.0124
10	−	f	4	10	9	+	f	3	8	2136.0604	2136.0738	−0.0134
10	+	e	4	11	9	−	e	3	10	2145.2285	2145.2524	−0.0239
10	+	e	5	9	9	−	e	4	8	2031.8406	2031.8191	0.0215
10	−	f	5	10	9	+	f	4	8	2041.0076	2040.9884	0.0192
...												
16	+	e	3	15	15	−	e	2	14	2271.8427	2271.8199	0.0228
16	−	f	3	16	15	+	f	2	14	2278.3547	2278.3273	0.0274
16	+	e	3	17	15	−	e	2	16	2284.1877	2284.1849	0.0028
16	+	e	4	15	15	−	e	3	14	2175.3368	2175.3445	−0.0077
17	−	e	1	16	16	+	e	0	15	2469.8998	2469.8935	0.0063
17	+	f	1	17	16	−	f	0	15	2476.8083	2476.8153	−0.0070
17	−	e	1	18	16	+	e	0	17	2483.0468	2483.0661	−0.0193
17	−	e	1	16	18	+	e	0	17	1930.5765	1930.5700	0.0065
17	+	f	1	17	18	−	f	0	17	1906.7108	1906.7114	−0.0006
17	−	e	1	18	18	+	e	0	19	1882.5218	1882.5467	−0.0249
17	−	e	2	16	16	+	e	1	15	2374.4089	2374.4329	−0.0240
17	+	f	2	17	16	−	f	1	15	2380.8107	2380.8373	−0.0266
17	−	e	2	18	16	+	e	1	17	2386.5164	2386.5774	−0.0610
17	−	e	3	16	16	+	e	2	15	2278.3547	2278.3206	0.0341
17	+	f	3	17	16	−	f	2	15	2284.1877	2284.1579	0.0298
17	−	e	3	18	16	+	e	2	17	2289.3440	2289.3366	0.0074
18	+	e	1	17	17	−	e	0	16	2476.8083	2476.7978	0.0105
18	−	f	1	18	17	+	f	0	16	2483.0468	2483.0481	−0.0013

Downloaded from https://academic.oup.com/mnras/article-abstract/488/2/2332/5529411 by UCL (University College London) user on 31 July 2019

Table 6. A comparison of experimental $a\,^1\Delta - X\,^3\Sigma^-$ (forbidden) frequencies (in cm^{-1}) from Beutel et al. (1996) (Obs.) with those calculated using DUO (Calc.).

J'	$\pm'$	e/f'	v'	N'	J''	$\pm''$	e/f''	v''	N''	Obs.	Calc.	Obs. − Calc.
2	+	e	0	2	3	−	e	0	4	7406.0737	7406.0727	0.0010
3	−	e	0	3	4	+	e	0	5	7372.6299	7372.6427	−0.0128
4	+	e	0	4	5	−	e	0	6	7339.3906	7339.3921	−0.0015
5	−	e	0	5	6	+	e	0	7	7306.3367	7306.3324	0.0043
6	+	e	0	6	7	−	e	0	8	7273.4977	7273.4805	0.0172
7	−	e	0	7	8	+	e	0	9	7240.8720	7240.8559	0.0161
8	+	e	0	8	9	−	e	0	10	7208.5009	7208.4794	0.0215
9	−	e	0	9	10	+	e	0	11	7176.3990	7176.3726	0.0264
2	−	f	0	2	3	+	f	0	2	7471.0723	7471.0815	−0.0092
3	+	f	0	3	4	−	f	0	3	7454.5009	7454.5073	−0.0064
4	−	f	0	4	5	+	f	0	4	7438.0317	7438.0375	−0.0058
5	+	f	0	5	6	−	f	0	5	7421.6792	7421.6832	−0.0040
6	−	f	0	6	7	+	f	0	6	7405.4577	7405.4557	0.0020
7	+	f	0	7	8	−	f	0	7	7389.3738	7389.3667	0.0071
8	−	f	0	8	9	+	f	0	8	7373.4400	7373.4278	0.0122
9	+	f	0	9	10	−	f	0	9	7357.6640	7357.6514	0.0126
2	+	e	0	2	2	−	f	0	1	7521.4973	7521.5055	−0.0082
3	−	e	0	3	3	+	f	0	2	7521.6843	7521.6904	−0.0061
4	+	e	0	4	4	−	f	0	3	7521.9341	7521.9375	−0.0034
5	−	e	0	5	5	+	f	0	4	7522.2483	7522.2477	0.0006
6	+	e	0	6	6	−	f	0	5	7522.6249	7522.6217	0.0032
7	−	e	0	7	7	+	f	0	6	7523.0669	7523.0608	0.0061
8	+	e	0	8	8	−	f	0	7	7523.5775	7523.5663	0.0112
9	−	e	0	9	9	+	f	0	8	7524.1112	7524.1400	−0.0288
10	+	e	0	10	10	−	f	0	9	7524.7853	7524.7841	0.0012
2	−	f	0	2	1	+	f	0	0	7555.1330	7555.1391	−0.0061
3	+	f	0	3	2	−	f	0	1	7572.1114	7572.1144	−0.0030
4	−	f	0	4	3	+	f	0	2	7589.1204	7589.1206	−0.0002
5	+	f	0	5	4	−	f	0	3	7606.1501	7606.1477	0.0024
6	−	f	0	6	5	+	f	0	4	7623.1921	7623.1862	0.0059
7	+	f	0	7	6	−	f	0	5	7640.2333	7640.2267	0.0066
8	−	f	0	8	7	+	f	0	6	7657.2646	7657.2604	0.0042
9	+	f	0	9	8	−	f	0	7	7674.2851	7674.2784	0.0067
10	−	f	0	10	9	+	f	0	8	7691.2735	7691.2726	0.0009
11	+	f	0	11	10	−	f	0	9	7708.2094	7708.2353	−0.0259
12	−	f	0	12	11	+	f	0	10	7725.1395	7725.1594	−0.0199
2	+	e	0	2	1	−	e	0	0	7573.5937	7573.6014	−0.0077
3	−	e	0	3	2	+	e	0	1	7607.7241	7607.7292	−0.0051
4	+	e	0	4	3	−	e	0	2	7641.7120	7641.7149	−0.0029
5	−	e	0	5	4	+	e	0	3	7675.6392	7675.6403	−0.0011
6	+	e	0	6	5	−	e	0	4	7709.5131	7709.5125	0.0006
7	−	e	0	7	6	+	e	0	5	7743.3243	7743.3220	0.0023
8	+	e	0	8	7	−	e	0	6	7777.0560	7777.0542	0.0018
9	−	e	0	9	8	+	e	0	7	7810.6816	7810.6924	−0.0108
10	+	e	0	10	9	−	e	0	8	7844.1942	7844.2194	−0.0252
10	−	f	0	10	11	+	f	0	10	7342.0698	7342.0500	0.0198

become important for high J, the vibrational kinetic energy operator for each state was extended by

$$-\frac{\hbar^2}{2\mu r^2} \rightarrow -\frac{\hbar^2}{2\mu r^2}\left(1 + g^{\mathrm{BOB}}(r)\right), \tag{5}$$

where the unitless X and a BOB functions were represented by the (unitless) polynomial $g^{\mathrm{BOB}}(r) = F(r)$. The X-state BOB function required a fourth-order expansion in terms of damped-z in equation (4), while for the a-stated only one C_0 constant from equation (3) was needed. When fitting to the experimental frequencies, we had to include other X-state correction terms, such as spin–spin and spin–rotation (see Yurchenko et al. 2016), for

Downloaded from https://academic.oup.com/mnras/article-abstract/488/2/2332/5529411 by UCL (University College London) user on 31 July 2019

which the same z-damped expression equation (3) was used, of third and zeroth orders, respectively. All expansion parameters are given in Table 2 and in the supplementary material as part of the DUO input file.

Experimental data were taken primarily from four sources. To determine the X-state curves, submillimetre-wave measurements of the ($N' = 0$, 1) rotational spectrum by Goto & Saito (1993) and the ($N' = 1$, 2) spectrum by Klisch et al. (1998) were combined with frequencies from an infrared (IR) Fourier transform spectrometer vibration–rotation spectrum of the ground state of PH by Ram & Bernath (1987). The infrared study observed five vibrational bands (1–0, 2–1, 3–2, 4–3, and 5–4) up to a maximum rotation state of $J = 21$. The X-state data set comprised 381 lines split among six fine-structure resolved branches: R_1, R_2, R_3, P_1, P_2, and P_3 that characterize the triplet pattern arising from the splitting of the lines from the electronic spin angular momentum along the internuclear axis (i.e. different spin projections $\Sigma = -1$, 0, 1; note that the X state is Hund's case (b) so these projections on the internuclear axis are not good quantum numbers). These data allowed the lowest six vibrational states ($v = 0 \ldots 5$) to be characterized. The hyperfine structure of the submillimetre-wave frequencies (Goto & Saito 1993; Klisch et al. 1998) was averaged. For the a-state, 64 a–X IR transition frequencies (0–0 band) from Beutel et al. (1996) were used.

According to Rumble (2018) (with the original reference to Luo 2007), the dissociation value for PH at $T = 298$ K is 297.0 ± 2.1 kJ mole^{-1} or 293.2 kJ mole^{-1} at 0 K (24 516 ± 175 cm^{-1} or 3.04(2) eV). Using a zero-point energy value of 1170 cm^{-1} from our calculations (ZPE $= D_e - D_0$), this corresponds to $D_e = 25\,687 \pm 175$ cm^{-1} (3.19 eV). The value $A_e(X) = D_e(X) = 25\,700$ cm^{-1} was adopted as the dissociation energy of the X-state in our calculations. Throughout the refinement phase, the equilibrium distance r_e was kept fixed at $r_e = 1.4221$ Å, as spectroscopically determined by Ram & Bernath (1987).

The dissociation channel for the a states can be estimated using the phosphorus atom excitation energy ($^2D_{3/2}$): $A_e(a) = D_e(X) + 11361.02 \approx 37000$ cm^{-1} (Kramida et al. 2019), which was used to constrain the dissociation energy of $a\,^1\Delta$ while varying the corresponding value of the origin V_e.

The PECs and other empirical curves fitted directly to experimental-measured frequencies ($J \leq 21$) achieved a root-mean-square error of 0.01 cm^{-1}. The final refined PECs are shown in Fig. 1 and empirical curves are shown in Fig. 2. Some of the residuals are illustrated in Tables 3–6.

2.2 *Ab initio* dipole moment curves

PH has a permanent dipole and can be represented by a dipole moment curve (DMC) that shows the variation of the dipole with internuclear separation. Gao & Gao (2014) computed an *ab initio* DMC for the $X\,^3\Sigma^-$ state of PH using an aug-ccpV5Z basis set at the MRCI+Q level of theory. We used the same method to compute the DMC for the $a\,^1\Delta$ state with the MOLPRO program (Werner et al. 2012). These DMCs are illustrated in Fig. 3. As expected for a neutral species, the dipole moments tend to zero at large bond lengths.

The $X\,^3\Sigma^-$ state *ab initio* dipole moment has an equilibrium value of 0.4771 D. This compares reasonably with other theoretical study equilibrium values. Müller & Woon (2013) calculated dipole moments at a number of theoretical levels, using a variety of basis sets. An AV5Z basis set at the coupled cluster (CCSD(T)) level of theory produced a dipole moment of 0.4410 D. Other studies at the configuration–interaction (CI) level calculated the dipole moment as 0.431 D (Senekowitsch et al. 1986) and 0.432 D (Park & Sun 1992). Meyer & Rosmus (1975) using the coupled electron pair approach (CEPA) produced a dipole moment of 0.481 D, which is closest to the value of Gao & Gao (2014) used for our line list calculations.

The DMCs were represented analytically using the damped-z expansion given by equation (3). This was done in order to reduce the numerical noise in the calculated intensities for high overtones; see recommendations by Medvedev et al. (2016). These DMCs and the empirically defined curves constitute our spectroscopic model, which was then used with DUO to produce a PH line list. The corresponding expansion parameters are listed in Table 7. They can also be found in the supplementary data in the form of the DUO input files together with the corresponding grid representations.

3 RESULTS

3.1 Line list

The spectroscopic model described in the previous sections was used to generate the line list for the ground (X) and first excited (a) electronic states of ^{31}PH. The LaTY line list was computed using the empirical PECs and correction curves and *ab initio* DMCs described above. All vibrational states up to $v = 17$ (X) and $v = 9$ (a), rotational states up to $J = 80$ and energies up to $D_0(X)$ were considered. A dipole moment cut-off of 10^{-7} D was applied. The zero-point energy was calculated to be 1170.47 cm^{-1} defined as the lowest state of the system ($J = 1$, $v = 0$, $N = 0$, $e(-)$) above the minimum of the X potential ($V_e = 0$ cm^{-1}). The final line list contains 2528 states and 65 055 transitions. These levels are sufficient to represent the ground state up to temperatures of about 4000 K, but at these temperatures electronically excited states should also be occupied giving rise to further transitions not considered here. The line list consists of the electric dipole transitions only. Moreover, the $X\,^3\Sigma^-$ and $a\,^1\Delta$ states are fully uncoupled and therefore the line list does not include the weak, forbidden $a - X$ transitions observed in Beutel et al. (1996).

The results are provided in the standard ExoMol format (Tennyson et al. 2016a) as states and transitions files, see extracts given in Tables 8 and 9, respectively. Since DUO works in Hund's case (a) but PH is a Hund's case (b) molecule for the X state, the (±, Λ, Σ, Ω) quantum numbers were converted to N, *e/f*. For the $a\,^1\Delta$ state, $N = J$, $\Sigma = 0$, $\Lambda = \Omega = 2$. Here N is the rotational quantum number defined as a projection of $\boldsymbol{N} = \boldsymbol{J} - \boldsymbol{S}$, where $\boldsymbol{J}$ and $\boldsymbol{S}$ are the total and spin angular momenta, respectively. The states file also gives Landé g-factors for the various states (Semenov, Yurchenko & Tennyson 2017) that can be used to model the behaviour of these states in a weak magnetic field.

3.2 Partition function

The partition function, $Q(T)$, was calculated by summing the energy levels given by DUO for temperatures up to $T = 4000$ K. ExoMol follows the HITRAN convention (Gamache et al. 2017) of explicitly including the full atomic nuclear spin in the molecular partition function via the nuclear spin statistical number g_{ns}. Since both P and H have nuclear spins 1/2, $g_{ns} = 4$.

The partition function at a range of temperatures is catalogued in Table 10. It was compared with sources where the partition function $Q(T)$ was deduced from polynomial approximations (Irwin 1981;

Downloaded from https://academic.oup.com/mnras/article-abstract/488/2/2332/5529411 by UCL (University College London) user on 31 July 2019

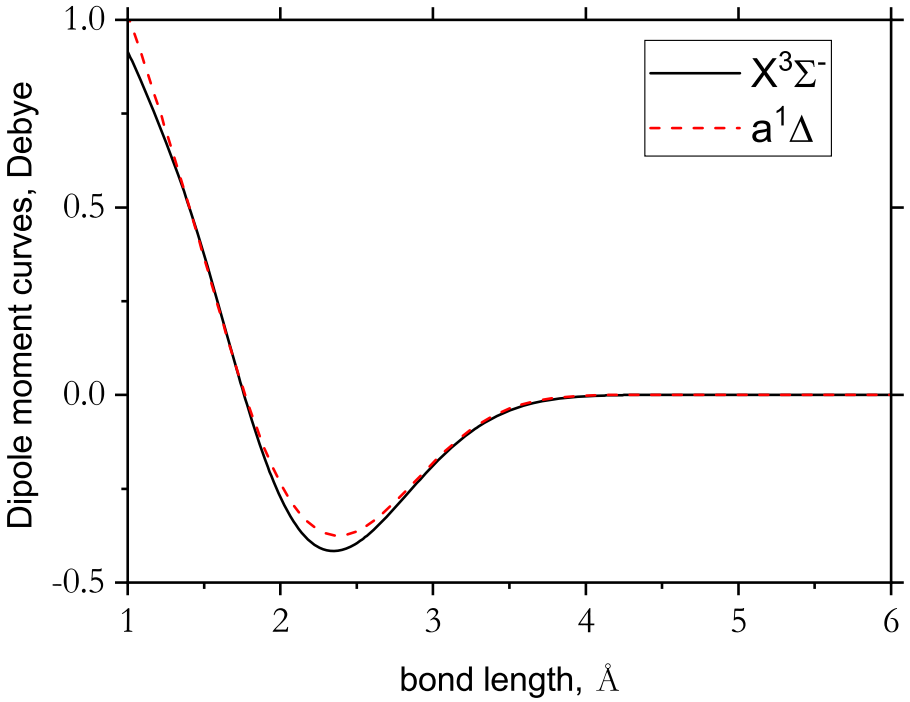

Figure 3. *Ab initio* PH MRCI+*Q*/AV5Z dipole moment curve (DMC) used in this work: the $X\,^3\Sigma^-$ state DMC is from Gao & Gao (2014), and $a\,^1\Delta$ DMC was computed as part of this study.

Table 7. Expansion parameters defining *X* and *a* DMCs according to equation (4). The units are Å (Angstrom) and D (Debye).

Parameters	DMC(*X*)	DMC(*a*)
$r_{\rm ref}$	1.4222	1.4222
γ_2	0.1695549437	0.1233507271
γ_4	0.0116033136	0.0210533244
p	6	6
D_0	0.4766434841	0.4747489601
D_1	− 0.2603505526	− 0.3886599811
D_2	− 1.6119565470	− 1.3959503273
D_3	− 4.4208750252	− 3.5580088368
D_4	− 3.6843015061	− 2.7131260560
D_∞	0	0

Sauval & Tatum 1984; Barklem & Collet 2016). The cited partition functions were all multiplied by 4 to match with the HITRAN convention adopted. It can be seen that all the sources approximately agree with each other between 1000 and 4000 K. Below 1000 K, polynomial representations of $Q(T)$ used by Sauval & Tatum (1984) and Irwin (1981) are not valid; our results are much closer to the modern values of Barklem & Collet (2016) albeit slightly higher probably because of our full treatment of electron spin effects. Above 4000 K our values for $Q(T)$ are lower than those of Sauval & Tatum (1984) and Barklem & Collet (2016); these works include the contribution from electronically excited states that we neglect.

3.3 Experimental spectra

Two vibration–rotation emission spectra were recorded with the Fourier transform spectrometer at the National Solar Observatory at Kitt Peak in Arizona. The first spectrum (Spectrum 1 shown as the upper red trace in Fig. 4; Ram & Bernath 1987) was recorded with an electrodeless quartz discharge tube excited with a 2450-MHz microwave oscillator. A mixture of 0.45 Torr of hydrogen and 0.04 Torr of white phosphorus vapour flowed through the cell. The spectral resolution was 0.02 cm^{-1} and covered the 1800–9000 cm^{-1} region. The second spectrum (Spectrum 2 shown as the lower green trace in Fig. 4) differed only in the gas mixture used: 2.75 Torr of helium, 0.04 Torr of white phosphorus, and 0.03 Torr of methane. Both spectra contained many molecules including CO, CH, PH, CP, P_2, ArH, CN, and C_2. The strongest interfering molecule overlapping PH is CO with its $\Delta v = 1$ emission lines. The CO lines were used for wavenumber calibration. The vibration–rotation emission lines of PH are stronger in the first spectrum but the number of interfering lines is somewhat reduced in the second spectrum. Norton–Beer strong apodization was used because the lines were not resolved at 0.02 cm^{-1} resolution and the lines still have residual 'ringing' from the instrument line shape function.

3.4 Theoretical spectra

Fig. 5 gives an overview of full PH spectrum in absorption at two temperatures, 300 and 2000 K. At the lower temperature a clear progression of vibrational bands can be seen that is substantially washed out at the higher temperature due to the presence of many more weak lines in the spectrum.

Fig. 6 shows the microwave spectrum of the ground state of PH at $T = 296$ K. It is compared with the Cologne Database for Molecular Spectroscopy (CDMS) spectrum (Müller et al. 2005) ($v = 0$), which we have averaged over the hyperfine components. The dipole moment used by CDMS is 0.396 D at r_e (Müller, unpublished work), whereas the dipole moment from this work is 0.477 D at equilibrium

Downloaded from https://academic.oup.com/mnras/article-abstract/488/2/2332/5529411 by UCL (University College London) user on 31 July 2019

Table 8. Sample extract of the states file for ^{31}PH.

i	$\tilde{E}$	g_i	J	g	$\pm$	e/f	State	v	N
73	16.481110	20	2	1.00004	+	e	X3Sigma-	0	1
74	100.157012	20	2	−0.66632	+	e	X3Sigma-	0	3
75	2292.186846	20	2	0.99997	+	e	X3Sigma-	1	1
76	2373.329250	20	2	−0.66625	+	e	X3Sigma-	1	3
77	4480.481941	20	2	0.99989	+	e	X3Sigma-	2	1
78	4559.093532	20	2	−0.66618	+	e	X3Sigma-	2	3
79	6581.109731	20	2	0.99981	+	e	X3Sigma-	3	1
80	6657.178701	20	2	−0.66610	+	e	X3Sigma-	3	3
81	7573.601437	20	2	0.66667	+	e	a1Delta	0	2
82	8593.416817	20	2	0.99974	+	e	X3Sigma-	4	1
83	8666.923664	20	2	−0.66602	+	e	X3Sigma-	4	3
84	9899.143295	20	2	0.66667	+	e	a1Delta	1	2
85	10516.156390	20	2	0.99966	+	e	X3Sigma-	5	1
86	10587.067513	20	2	−0.66594	+	e	X3Sigma-	5	3

Note. i: state counting number.
$\tilde{E}$: state energy in cm^{-1}.
g_i: total statistical weight, equal to $g_{\rm ns}(2J+1)$.
J: total angular momentum.
g: Landé g-factors.
e/f: rotationless parity.
$\pm$: total parity.
State: electronic state.
v: state vibrational quantum number.
N: rotational quantum number; $\boldsymbol{N} = \boldsymbol{J} - \boldsymbol{S}$ ($\boldsymbol{S}$ is spin).

Table 9. Sample extract of the transitions file for ^{31}PH.

f	i	A_{fi}	$\tilde{\nu}_{fi}$
100	134	2.1325E-06	31.942920
162	135	3.0255E-05	31.959112
102	60	2.8977E-05	32.215418
256	285	3.2537E-06	32.223799
44	4	1.7832E-04	32.237083
174	75	6.7300E-04	32.439634
121	79	8.4497E-05	32.564436
119	20	5.1188E-04	32.625072
2047	2069	1.1922E-11	32.678476

Note. f: state number of final state.
i: state number of initial state.
A_{fi}: Einstein A coefficient.
$\tilde{\nu}_{fi}$: transition wavenumber.

or, more importantly, our $v = 0$ state vibrationally averaged dipole is 0.4499 D. This disparity can be seen in the graph, with our lines being more intense due to the larger dipole moment. Partition function values from CDMS agree with that from this work. At 300 K, the CDMS value was 302.12, while our value is 302.14. The line strength depends on the dipole moment squared. With this in mind, our intensities are about 1.27 times higher than those given by CDMS. We suggest that CDMS may wish to rescale their intensity values to ours. Conversely, the CDMS frequencies rely directly on data taken in the same frequency region and include the hyperfine components and must be considered more accurate than ours in this region; they should be used for any attempts to detect PH in the interstellar medium.

Fig. 4 compares the IR rovibrational experimental spectra from Ram & Bernath (1987) with calculations from this work. We assumed the non-local thermodynamic equilibrium (LTE) model based on two temperatures, rotational $T_{\rm rot}$ and vibrational $T_{\rm vib}$, as implemented in DUO. The temperatures were adjusted to match the experimental emission spectra of PH, with the final values of 800 and 2300 K, respectively. The grey vertical line indicates the experimental line positions from Ram & Bernath (1987). The good agreement with the observed spectrum of Ram & Bernath (1987) is found across the entire region and confirms the accuracy of our calculations.

4 CONCLUSION

A comprehensive line list for the ground (X) and first excited (a) electronic states of ^{31}PH, known as LaTY, is presented. It is based on an accurate PECs, BOB, SS, and SR curves obtained by fitting to a set of experimental transition line frequencies and extrapolating to higher rovibrational levels and *ab initio* DMCs. Future work can include analysis and investigations of higher electronic states of PH with the aim of creating a line list appropriate at shorter wavelengths. Previous studies on the low-lying $b^1\Sigma^+$ of PH (Di Stefano et al. 1978, 1999; Xuan et al. 1978) and on the strongly dipole-allowed

Downloaded from https://academic.oup.com/mnras/article-abstract/488/2/2332/5529411 by UCL (University College London) user on 31 July 2019

Table 10. Comparison with calculated partition functions, $Q(T)$, of Sauval & Tatum (1984), Irwin (1981), and Barklem & Collet (2016).

T (K)	This work	Sauval & Tatum	Irwin	Barklem & Collet
100	103.24	112.20	12.03	103.33
200	202.58	222.11	125.10	202.68
300	302.14	320.89	261.37	302.25
400	401.99	416.37	383.16	
500	502.54	512.03	494.35	502.64
600	604.56	609.72	600.96	
700	708.99	710.52	706.92	709.08
800	816.74	815.16	814.60	
900	928.57	924.17	925.49	
1000	1045.12	1037.97	1040.52	1045.20
1500	1713.31	1689.58	1694.33	1713.48
2000	2549.16	2501.19	2499.05	2550.26
2500	3580.45	3500.15	3467.86	
3000	4834.19	4713.74	4609.02	4847.12
4000	8112.16	7901.37	7436.84	8180.60

$A\,^3\Pi - X\,^3\Sigma^-$ system (Fitzpatrick et al. 2002, 2003; Gao & Gao 2014) in the near-ultraviolet provide a good starting point for future analysis of the PH molecule.

The line list can be downloaded from the CDS, via ftp://cdsarc.u-strasbg.fr/pub/cats/J/MNRAS/, or http://cdsarc.u-strasbg.fr/viz-bin/qcat?J/MNRAS/, or from www.exomol.com.

ACKNOWLEDGEMENTS

This work was supported by the UK Science and Technology Research Council (STFC) No. ST/R000476/1 and the COST action MOLIM No. CM1405. This work made extensive use of UCL's Legion high performance computing facility along with the STFC DiRAC HPC facility supported by BIS National E-infrastructure capital grant ST/J005673/1 and STFC grants ST/H008586/1 and ST/K00333X/1. Some support was provided by the NASA Laboratory Astrophysics Program.

REFERENCES

Ashfold M. N. R., Dixon R. N., Stickland R. J., 1984, Chem. Phys. Lett., 111, 226
Barklem P. S., Collet R., 2016, A&A, 588, A96
Beutel M., Setzer K. D., Shestakov O., Fink E. H., 1996, Chem. Phys. Lett., 249, 183
Bruna P. J., Hirsch G., Peyerimhoff S. D., Buenker P. J., 1981, Mol. Phys., 42, 875
Cui D., Tian F., Wang Y., Li C., Yu C., Yu L., 2017, Astrobiology, 17, 1219
Curry J., Herzberg L., Herzberg G., 1933, J. Chem. Phys., 1, 749
Davies P. B., Russell D. K., Thrush B. A., 1975, Chem. Phys. Lett., 36, 280
Di Stefano G., Lenzi M., Margani A., Xuan C. N., 1978, J. Chem. Phys., 68, 959
Di Stefano G., Lenzi M., Ricci A., 1999, Chem. Phys. Lett., 246, 267
Droege A., Engelking P., 1984, J. Chem. Phys., 80, 5926
Fitzpatrick J. A. J., Chekhlov O. V., Morgan D. R., Burrows R. W., Western C. M., 2002, Phys. Chem. Chem. Phys., 4, 1114
Fitzpatrick J. A. J., Chekhlov O. V., Western C. M., Ashworth S. H., 2003, J. Chem. Phys., 118, 4539
Gamache R. R. et al., 2017, J. Quant. Spectrosc. Radiat. Transf., 203, 70
Gao Y., Gao T., 2014, Spectrochim. Acta A, 118, 308
Goto M., Saito S., 1993, Chem. Phys. Lett., 211, 443
Guelin M., Cernicharo J., Paubert G., Turner B. E., 1990, A&A, 230, L9
Gustafsson O., Kindvall G., Larsson M., Senekowitsch J., Sigray P., 1985, Mol. Phys., 56, 1369
Hjalmarson A., Bergman P., Biver N., 2004, Adv. Space Res. J., 36, 1031
Hollis J. M., Snyder L. E., Lovas F. J., Ulich B. L., 1980, ApJ, 241, 158
Hughes R. A., Brown J. M., 1997, J. Mol. Spectrosc., 185, 197
Irwin A. W., 1981, ApJS, 45, 621
Ishaque M., Pearse R. W. B., 1939, Proc. R. Soc. Lond. Ser. A, 173, 0265
Jie-Min W., Jin-Feng S., De-Heng S., Zun-Lue Z., Wen-Tao L., 2012, Acta Phys. Sin., 61, 063104
Klisch E., Klein H., Winnewisser G., Herbst E., 1998, Z. Naturforschung A, 53, 733
Kramida A., Ralchenko Yu., Reader J., NIST ASD Team, 2019, NIST Atomic Spectra Database (ver. 5.6.1). National Institute of Standards and Technology, Gaithersburg, MD [Online]. Available: https://physics.nist.gov/asd [2019 April 13]
Le Roy R. J., 2017, J. Quant. Spectrosc. Radiat. Transf., 186, 167
Luo Y. R., 2007, Comprehensive Handbook of Chemical Bond Energies, 1st edn. CRC Press, Boca Raton, FL
Macia E., 2005, Chem. Soc. Rev., 34, 691
Medvedev E. S., Meshkov V. V., Stolyarov A. V., Ushakov V. G., Gordon I. E., 2016, J. Mol. Spectrosc., 330, 36
Meyer W., Rosmus P., 1975, J. Chem. Phys., 63, 2356
Millar T. J., 1991, A&A, 242, 241
Müller H. S. P., Woon D. E., 2013, J. Phys. Chem. A, 117, 13868
Müller H. S. P., Schlöder F., Stutzki J., Winnewisser G., 2005, J. Mol. Structure, 742, 215
Ohashi N., Kawaguchi K., Hirota E., 1984, J. Mol. Spectrosc., 103, 337
Park J. K., Sun H., 1992, Chem. Phys. Lett., 195, 469
Pearse R. W. B., Fowler A., 1930, Proc. R. Soc. Lond. Ser. A, 129, 328
Prajapat L., Jagoda P., Lodi L., Gorman M. N., Yurchenko S. N., Tennyson J., 2017, MNRAS, 472, 3648
Ram R. S., Bernath P. F., 1987, J. Mol. Spectrosc., 122, 275
Ram R. S., Bernath P. F., 1996, J. Mol. Spectrosc., 176, 329
Rao T. V. R., Reddy R. R., Rao P. S., 1981, Physica B+C, 106, 445
Rostas J., Cossart D., Bastien J. R., 1974, Can. J. Phys., 52, 1274
Rumble J., 2018, CRC Handbook of Chemistry and Physics, 99th edn. CRC Press, Boca Raton, FL
Sauval A. J., Tatum J. B., 1984, ApJS, 56, 193

Downloaded from https://academic.oup.com/mnras/article-abstract/488/2/2332/5529411 by UCL (University College London) user on 31 July 2019

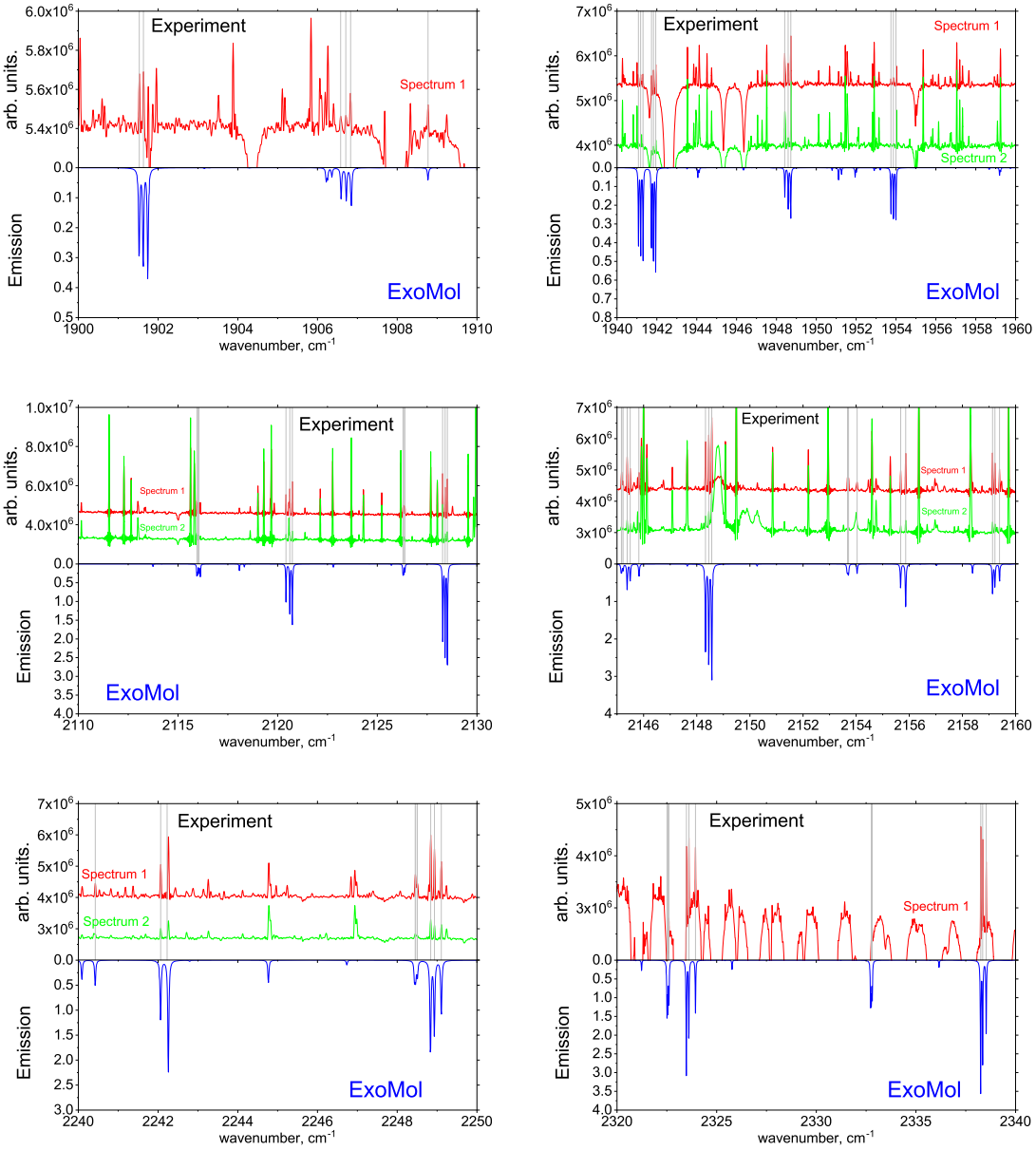

Figure 4. Experimental infrared spectra (see text for details) of the $X\,^3\Sigma^-$ state of PH compared to the ExoMol emission (photons s^{-1}) at $T_{\rm rot} = 800$ K and $T_{\rm vib} = 2300$ K using a Voigt line profile with $\gamma = 0.15$ cm^{-1}. Vertical grey lines indicate experimental line positions from Ram & Bernath (1987).

Semenov M., Yurchenko S. N., Tennyson J., 2017, J. Mol. Spectrosc., 330, 57

Senekowitsch J., Rosmus P., Werner H. J., Larsson M., 1986, Z. Naturforschung A, 41, 719

Shi D., Xing W., Sun J., Zhu Z., Liu Y., 2012, J. Mol. Spectrosc., 276, 1

Sousa-Silva C., Al-Refaie A. F., Tennyson J., Yurchenko S. N., 2015, MNRAS, 446, 2337

Tenenbaum E. D., Woolf N. J., Ziurys L. M., 2007, ApJ, 666, L29

Tennyson J., 2012, WIREs Comput. Mol. Sci., 2, 698

Tennyson J., Yurchenko S. N., 2012, MNRAS, 425, 21

Tennyson J., Yurchenko S. N., 2017, Mol. Astrophys., 8, 1

Tennyson J. et al., 2016a, J. Mol. Spectrosc., 327, 73

Tennyson J., Lodi L., McKemmish L. K., Yurchenko S. N., 2016b, J. Phys. B: At. Mol. Opt. Phys., 49, 102001

Thorne L. R., Anicich V. G., Prasad S. S., Huntress W. T.,, Jr, 1984, ApJ, 280, 139

Visscher C., Lodders K., Fegley B.,, Jr, 2006, ApJ, 648, 1181

Werner H.-J., Knowles P. J., Knizia G., Manby F. R., Schütz M., 2012, WIREs Comput. Mol. Sci., 2, 242

Xuan C. N., di Stefano G., Lenzi M., Margani A., Mele A., 1978, Chem. Phys. Lett., 57, 207

Yorke L., Yurchenko S. N., Lodi L., Tennyson J., 2014, MNRAS, 445, 1383

Yurchenko S. N., Lodi L., Tennyson J., Stolyarov A. V., 2016, Comput. Phys. Commun., 202, 262

Yurchenko S. N., Sinden F., Lodi L., Hill C., Gorman M. N., Tennyson J., 2018, MNRAS, 473, 5324

Zerkle A. L., 2018, Philos. Trans. R. Soc. A, 376, 20170401

Downloaded from https://academic.oup.com/mnras/article-abstract/488/2/2332/5529411 by UCL (University College London) user on 31 July 2019

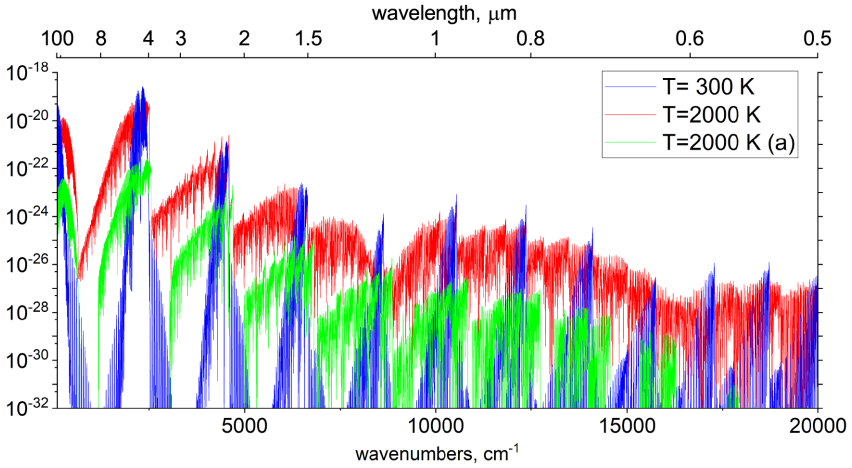

Figure 5. Absorption spectrum of PH at different temperatures computed using ExoMol line list and a Gaussian line profile of 2 cm^{-1}. The contribution from the a-band at $T = 2000$ K is shown separately.

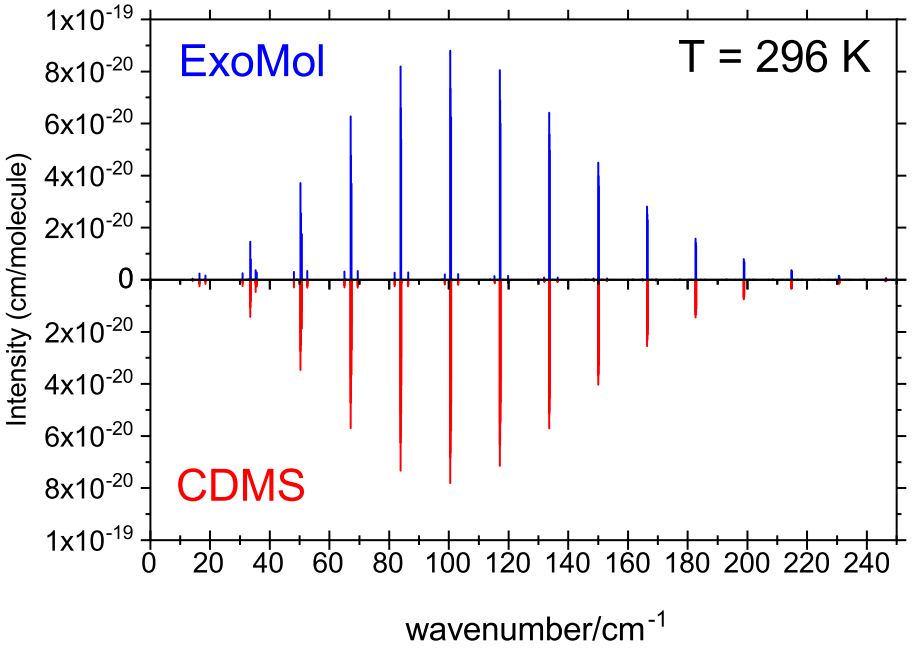

Figure 6. Pure rotational band within $v = 0$ for the rovibrational absorption stick spectra of the $X\,^3\Sigma^-$ state of PH at 296 K.

Ziurys L. M., 1987, ApJ, 321, L81

SUPPORTING INFORMATION

Supplementary data are available at *MNRAS* online.

PH.pf
PH.states
PH_model.inp

Please note: Oxford University Press is not responsible for the content or functionality of any supporting materials supplied by the authors. Any queries (other than missing material) should be directed to the corresponding author for the article.

This paper has been typeset from a TEX/LATEX file prepared by the author.

Downloaded from https://academic.oup.com/mnras/article-abstract/488/2/2332/5529411 by UCL (University College London) user on 31 July 2019